

***IMPROVED QUANTIFICATION OF THE FIRST AEROSOL INDIRECT  
EFFECT FROM SATELLITE***

H. Shao, G. Liu, and Y. Liu

*Submitted to  
Nature*

October 2006

**Environmental Sciences Department/Atmospheric Sciences Division**

**Brookhaven National Laboratory**

P.O. Box 5000  
Upton, NY 11973-5000  
[www.bnl.gov](http://www.bnl.gov)

## **DISCLAIMER**

This report was prepared as an account of work sponsored by an agency of the United States Government. Neither the United States Government nor any agency thereof, nor any of their employees, nor any of their contractors, subcontractors, or their employees, makes any warranty, express or implied, or assumes any legal liability or responsibility for the accuracy, completeness, or any third party's use or the results of such use of any information, apparatus, product, or process disclosed, or represents that its use would not infringe privately owned rights. Reference herein to any specific commercial product, process, or service by trade name, trademark, manufacturer, or otherwise, does not necessarily constitute or imply its endorsement, recommendation, or favoring by the United States Government or any agency thereof or its contractors or subcontractors. The views and opinions of authors expressed herein do not necessarily state or reflect those of the United States Government or any agency thereof.

# Improved quantification of the first aerosol indirect effect from satellite

Hongfei Shao<sup>1</sup>, Guosheng Liu<sup>1</sup>, and Yangang Liu<sup>2</sup>

<sup>1</sup>*Department of Meteorology, Florida State University, Tallahassee, 32306, USA*

<sup>2</sup>*Atmospheric Sciences Division, Brookhaven National Laboratory, New York 11973, USA*

**Anthropogenic aerosols enhance cloud reflectance of solar radiation by increasing the number concentration of cloud droplets that form on aerosols<sup>1</sup>. This process is referred to as the first aerosol indirect effect (AIE), and acts to substantially offset the warming caused by greenhouse gases. However, the first AIE is poorly quantified, which in turn leads to large uncertainties in the sensitivity of climate to changing greenhouse gas concentrations<sup>2</sup>. Here we show from analysis of satellite data that model parameterization of aerosol-cloud interactions based on local/regional measurements of the relation between cloud drop and aerosol number concentrations does not represent the real process of the first AIE, because these measurements implicitly contain a term associated with the co-variation of aerosol concentration and entrainment/mixing processes in clouds, thereby leading to large errors in calculation of aerosol radiative forcing. Removal of this mixing-aerosol correlation term reduces the global mean value and the uncertainties of the first AIE to about half of those recently published. This finding also explains the disparity between forward and inverse model estimates of indirect aerosol forcing<sup>3</sup>.**

The forcings that drive long-term climate change have not been understood well enough to forecast future climate. One of the problems is that the first AIE is not well

constrained in global climate models. Using currently accepted upper limit of the first AIE, the equilibrium response of global mean temperature to an equivalent doubling of CO<sub>2</sub> concentration (called climate sensitivity) was estimated by models as high as 10 K<sup>4, 5</sup>. However, the accepted climate sensitivity is likely in the range of 1.5 – 4.5 K<sup>6</sup>. Additionally, a systematic disparity among models exists for the aerosol-induced cooling tendency, termed as the indirect aerosol forcing. On average, forward model calculations of the indirect aerosol forcings are stronger than those inversely inferred from the total forcing required to match climate model simulations with observed temperature changes (–1.5 vs. –1.0 Wm<sup>–2</sup>), and are more than twice uncertain than those from the inverse calculations as well<sup>3</sup>. By constraining the predictions of climate models with satellite observations, it was found that the aerosol-induced cooling effect was overestimated by models likely due to the improper parameterization of the relationship between aerosol number concentration ( $N_a$ ) and cloud droplet number concentration ( $N_c$ )<sup>7, 8</sup>.

It has been recently shown that an increase of aerosol loading leads to concurrent increases of droplet concentration and relative dispersion of the cloud droplet size distribution, and that in contrast to the enhanced droplet concentration, the enhanced dispersion leads to a warming dispersion effect on climate<sup>9</sup>. Therefore, the first AIE should be a sum of the two competing effects arising from the change in droplet concentration and relative dispersion. Subsequent general circulation model (GCM) studies<sup>10, 11</sup> have further shown that although the dispersion effect offsets some cooling, the reduction is not enough to reconcile the GCM estimates with those constrained by observations. Using satellite observations over the Northeast Pacific near California coast, our recent study<sup>12</sup> showed that the observed correlation between  $N_c$  and  $N_a$  does not represent the  $N_c$ 's direct response to the change in  $N_a$  (as required in the GCM parameterization) unless all the clouds observed are subject to entrainment/mixing evaporation with ambient dry air uniformly. Otherwise, a correlation term arising from

the spatial co-variation between the mixing evaporation and the aerosol concentration is included. Because of its high sensitivity to the relation between  $N_c$  and  $N_a$ <sup>13-15</sup>, the aerosol indirect forcing calculated using the correlation term-tinted  $N_c - N_a$  relation is therefore in error. Is this correlation term responsible for the aforementioned inconsistencies among global model estimates? Motivated by this question, here we evaluate the first AIE unbiased by the correlation term using satellite observations on near-global scale.

During June, July and August (JJA), stratocumulus clouds frequently occur on the eastern side of the subtropical oceans, providing the best opportunity to observe the first AIE on large scale. In this study, satellite observations over the North-eastern Pacific (NEP), the South-eastern Pacific (SEP), the North-eastern Atlantic (NEA), and the South-eastern Atlantic (SEA) during JJA of 2000 to 2002 (Fig. 1) are utilized to evaluate the first AIE with and without the correlation term by  $IE_L$  and  $IE_H$ , respectively<sup>12</sup>, (see also Supplementary Information) i.e.,

$$IE_L = -\frac{\Delta \ln(r_e L^{-1/3})}{\Delta \ln \tau_a} \text{ and } IE_H = -\frac{\Delta \ln(r_e H^{-1/3})}{\Delta \ln \tau_a}, \quad (1)$$

where,  $r_e$  is cloud effective radius,  $\tau_a$  aerosol optical thickness,  $H$  cloud geometric thickness, and  $L$  liquid water content at cloud top;  $\Delta$  means taking difference between clean and polluted clouds. In non-precipitating stratocumulus clouds  $r_e$  is related to droplet number concentration through  $r_e \propto \omega L^{1/3} N_c^{-1/3}$ , where  $\omega$  is a non-dimensional parameter depicting the dispersion of cloud drop spectrum. Note that  $\tau_a$  is here used as a proxy of  $N_a$ .  $IE_L$  is equivalent to  $1/3(\Delta \ln N_c / \Delta \ln N_a)$  minus the dispersion effect<sup>9, 12</sup> (i.e.,  $\Delta \ln \omega / \Delta \ln N_a$ ).

In Fig.2, we compare  $IE_H$ ,  $IE_L$  and AIEs from in situ measurements published by previous investigators<sup>13, 16-23</sup>. Remarkably, the uncertainty in  $IE_H$  (Fig. 2a) is greatly

reduced to only about half of those AIEs containing the correlation term (Figs. 2b and 2c). Also reduced is the contrast of the first AIEs between northern and southern hemispheres. On the other hand, the first AIEs with the correlation term have comparable uncertainty despite the different methods and data used. It is also noticed that there is about a 0.1 difference in the means between satellite and in situ measurements. This difference, also reported in other satellite observations<sup>24</sup>, is likely due to the aforementioned dispersion effect<sup>9</sup> and the lack of measurements from the southern subtropical oceans, where, as we show later, the correlation term usually weakens the observed first AIE.

To understand the physics underlying the above results, we investigate the sign and the magnitude of the correlation term. For non-precipitating stratocumulus, because  $H$  is proportional to the maximum liquid water content at cloud top<sup>25</sup>, the ratio  $R=L/H$  can be used as a measure of the degree of mixing evaporation. It is seen from Fig.3 that the correlation between  $\ln R$  and  $\ln \tau_a$  is contingent on location and time: the strongest positive correction is found in NEP and the strongest negative correction is found in SEA. For SEP and NEA, the sign of the correlation changes from year to year. Consequently, as show in Fig.4,  $IE_L$  positively deviates from  $IE_H$  in NEP and negatively deviates from  $IE_H$  in NEP; the range of  $IE_L$  is therefore broader than that of  $IE_H$ . The insensitivity of  $IE_H$  to  $\Delta \ln R / \Delta \ln \tau_a$  confirms that  $IE_H$  measures the first AIE approximately without containing the correlation term. It is noticed that although local measurements of  $IE_L$  can be biased largely in either directions, the difference between averaged  $IE_H$  and  $IE_L$  is rather small (Fig. 2) because of the cancellation of positive and negative correlation terms.

In GCMs, the indirect aerosol forcings are calculated from an empirical relationship between  $N_c$  and  $N_a$  based on local measurements that implicitly include mixing influences. If this measurement occurs in the regions where  $R$  positively co-varies with aerosol

loading, because the correlation term enhances the observed first AIE in this case, the upper limit of the first AIE will be overestimated. According to our measurements of  $IE_L$  in the North-eastern Pacific, plus the dispersion effect (approximately 0.04 on average<sup>10-12</sup>), we may deduce that the first AIE measured by  $\frac{1}{3}(\Delta \ln N_c / \Delta \ln N_a)$  can be as large as 0.24, whereas the real strength of the AIE estimated from  $IE_H$  is only around 0.1. Based on Boucher and Lohmann model results<sup>13</sup>, we relate  $\frac{1}{3}(\Delta \ln N_c / \Delta \ln N_a)$  to indirect aerosol forcing in  $\text{W m}^{-2}$  as shown by the scale on the right side of in Fig.2. Reading from it, our measurements of  $IE_H$  can be translated into the aerosol indirect forcing ranging from -0.4 to  $-1.0 \text{ W m}^{-2}$ , consistent with the range of 0 to  $-1.2 \text{ W m}^{-2}$  estimated inversely from historical climate record data coupled with a simple climate model<sup>2</sup>. In other words, the uncertainties in forward model calculations of aerosols indirect forcing would be reduced by half if proper parameterization of aerosol-cloud interactions such as using the AIE value derived from this study were used. Recalling that uncertainties in inverse model calculations being about half of those in forward model calculations<sup>3</sup>, the uncertainties in the aerosol indirect forcing from forward model calculations can be therefore reconciled with those from inverse model calculations by removing the correlation term contained in early estimates of the AIE. Note also that the AIEs with the correlation term are positively biased in NEP and negatively biased in SEA. This partially explains the contrast of the indirect aerosol forcing between the north and south hemisphere<sup>13</sup>.

Due to the different sensitivity of  $IE_H$  and  $IE_L$  to mixing, theoretically  $IE_H$  equals to  $IE_L$  only when mixing evaporation (i.e.,  $\Delta \ln R / \Delta \ln \tau_a$ ) is null. Therefore, the cross point of the best-fitting lines in Fig. 4 represents the mean first AIE unbiased by the mixing-aerosol correlation term and is independent of measuring locations (see detail in Supplementary Information). Our data show that the global mean first AIE is around 0.1 with 95% confidence interval of less than 0.03 (Fig. 4). Comparing to averaged  $IE_L$  (0.08), the "global" mixing influence is negligibly weak, although locally it can be quite

strong in either directions. Since empirical parameterizations are based on fitting data observed locally/regionally, the large uncertainties in forward calculations in fact reflects the variability of the mixing-aerosol co-variation, not uncertainty in global mean first AIE as conventionally thought.

In short, our work has the following important implications. First, the claimed inconsistency among estimates of the first AIE is primarily caused by the correlation term that has been implicitly included in most forward estimates by climate models. Removing this correlation term, the observed values are fairly consistent from year to year and from place to place. Second, our estimate of the first AIE corroborates the inverse model calculations of indirect aerosol forcing, which further suggests that forward model calculations may have overestimated the indirect cooling effect of aerosols on climate due to improper parameterization of the relationship between aerosol loading and cloud radiative properties. Third, the upper limit of the first AIE has been overestimated due to the correlation term. The large climate sensitivity ( $> 10$  K) based on previous estimates is unrealistic. By referring to earlier simple climate model results<sup>5</sup>, our estimate of the first AIE suggests that climate sensitivity is no excess to 3.0 K, therefore indicates a milder climate change in the future.

## **Methods**

In this study, clouds effective radius, optical depth, liquid water path, and drizzle index are derived from the Tropical Rainfall Measurement Mission (TRMM) satellite data during JJA of 2000 to 2002<sup>26</sup>. Six-hourly NCEP/NCAR (National Center for Environmental Prediction / National Center for Atmospheric Research) reanalysis surface data combined with TRMM thermal channel data are utilized to obtain geometric cloud thickness<sup>27</sup>. Data of aerosol optical depth are from the Moderate Resolution Imaging

Spectroradiometer orbital aerosol optical depth product (MOD04\_L2). To ensure that measurements are from warm, non-precipitating and single-layer stratocumulus, we use the following strict criteria to refine our dataset: 1) infrared cloud top temperature warmer than 280 K, 2) cloud effective radius between 8 and 16  $\mu\text{m}$ , 3) liquid water path ( $W$ ) between 20 and 400  $\text{g m}^{-2}$ , 4) cloud geometric thickness ( $H$ ) between 250 and 850 m, 5)  $WH^2$  between 100 and 500  $\text{g m}^{-2} \text{km}^{-2}$ , 6) the absolute value of drizzle index less than 1.0, and 7) the product of the variances of cloud effective radius and optical depth within a TRMM Microwave Imager's 37 GHz field of view ( $\sim 12 \text{ km}$ ) less than  $8.0 \mu\text{m}^2$  (a threshold used to filter out non-uniform convective clouds). In addition to these criteria, only data with solar zenith angle  $< 60^\circ$  and satellite zenith angle  $< 35^\circ$  are used to further avoid "3D effect" on cloud property retrievals. After the dataset are selected, three-monthly geometric means within  $1^\circ$  by  $1^\circ$  grid are performed to represent the mean states of aerosol and clouds (Fig .1). Using mean data, linear regressions (Figs. 3, S1, and S2) are performed to obtain  $\Delta \ln R / \Delta \ln \tau_a$ ,  $IE_L$ , and  $IE_H$  based on the following models:

$$\ln Y \sim \ln \tau_a \text{ (for NEP only)}$$

$$\ln Y \sim (\ln \tau_a, n)$$

where,  $n$  is a nominal variable.  $n = 1$  when  $\tau_a > 0.15$ , otherwise  $n = 0$ ;  $Y$  denotes either  $LH^1$  or  $-r_e L^{-1/3}$  or  $-r_e H^{1/3}$ . Note that  $L$  here is inferred from  $2WH^1$  because liquid water content in stratocumulus clouds increases generally linearly with height. To avoid the influence of some outliers, we do regression twice. The second regressions are performed after the data points with residual for the first regression greater than 0.18 are discarded.

## References

1. Twomey, S.A. The influence of pollution on the short wave albedo of clouds. *J. Atmos. Sci.* **34**, 1149-1152 (1977).
2. Knutti, R., Stocker, T.F., Joos, F. & Plattner, G.-K. Constraints on radiative forcing and future climate change from observations and climate model ensembles. *Nature* **416**, 719-723 (2002).
3. Anderson, T.L. et al. Climate forcing by aerosols—A hazy picture. *Science* **300**, 1103–1104 (2003).
4. Stainforth, D.A. et al. Uncertainty in predictions of the climate response to rising levels of greenhouse gases. *Nature* **433**, 403-406 (2005).
5. Andreae, M.O., Jones, C.D. & Cox, P.M. Strong present-day aerosol cooling implies a hot future. *Nature* **435**, 1187-1190 (2005).
6. Houghton, J. T. et al. in *Climate Change 2001: The Scientific Basis*. (Cambridge University Press, UK/New York, NY, 2001).
7. Lohmann, U. & Lesins, G. Stronger constraints on the anthropogenic indirect aerosol effect. *Science* **298**, 1012-1015 (2002).
8. Quaas, J. & Boucher, O. Constraining the first aerosol indirect radiative forcing in the LMDZ GCM using POLDER and MODIS satellite data. *Geophysical Research Letters* **32**, doi:10.1029/2005GL023850 (2005).
9. Liu, Y. & Daum, P.H. Indirect warming effect from dispersion forcing. *Nature* **419**, 580-581 (2002).
10. Rotstayn, L.D. & Liu, Y. Sensitivity of the First Indirect Aerosol Effect to an Increase of Cloud Droplet Spectral Dispersion with Droplet Number Concentration. *J. Climate* **16**, 3476-3481 (2003).
11. Peng, Y. & Lohmann, U. Sensitivity study of the spectral dispersion of the cloud droplet size distribution on the indirect aerosol effect. *Geophys. Res. Lett.* **30**, doi:10.1029/2003GL017192 (2003).
12. Shao, H. & Liu, G. Influence of Mixing on Evaluation of the Aerosol First Indirect Effect. *Geophys. Res. Letts.* **33**, doi:10.1029/2006GL026021 (2006).
13. Boucher, O. & Lohmann, U. The sulfate-CCN-cloud albedo effect. *Tellus* **47B**, 281-300 (1995).
14. Jones, A. & Slingo, A. Predicting cloud-droplet effective radius and indirect sulphate aerosol forcing using a general circulation model. *Quarterly Journal of the Royal Meteorological Society* **122**, 1573-1595 (1996).

15. Kiehl, J.T., Schneider, T.L., Rasch, P.J., Barth, M.C. & Wong, J. Radiative forcing due to sulfate aerosols from simulations with the National Center for Atmospheric Research Community Climate Model, Version 3. *J. Geophys. Res.* **105**, 1441–1457 (2000).
16. Raga, G.B. & Jonas, P.R. On the link between cloud-top radiative properties and sub-cloud aerosol concentrations. *Q. J. R. Meteorol. Soc.* **119**, 1419–1425 (1993).
17. Jones, A., Roberts, D.L. & A., S. A climate model study of indirect radiative forcing by anthropogenic sulfate aerosols. *Nature* **370**, 450-453 (1994).
18. Leaitch, W.R. et al. Physical and chemical observations in marine stratus during the 1993 North Atlantic Regional Experiment: Factors controlling cloud droplet number concentrations. *J. Geophys. Res.* **101**, 29123-29136 (1996).
19. Hegg, D.A. Cloud condensation nucleus-sulfate mass relationship and cloud albedo. *J. Geophys. Res.* **99**, 25903-25908 (1994).
20. Chuang, P.Y. et al. CCN measurements during ACE-2 and their relationship to cloud microphysical properties. *Tellus* **52B**, 843-867 (2000).
21. Feingold, G., Remer, L.A., Ramaprasad, J. & Kaufman, Y. Analysis of smoke impact on clouds in Brazilian biomass burning regions: An extension of Twomey's approach. *J. Geophys. Res.* **106**, 22,907-922,922 (2001).
22. Kaufman, Y.J., Fraser, R.S. & Mahoney, R.L. Fossil fuel and biomass burning effect on climate - Heating or cooling? *J. Climate* **4**, 578-588 (1991).
23. Twohy, C.H. et al. Evaluation of the aerosol indirect effect in marine stratocumulus clouds: Droplet number, size, liquid water path, and radiative impact. *J. Geophys. Res.* **110**, D08203 doi:08210.01029/02004JD005116 (2005).
24. Bréon, F.M., Tanre, D. & Generoso, S. Aerosol effect on cloud droplet size monitored from satellite. *Science* **295**, 834-838 (2002).
25. Brenguier, J.L. et al. Radiative properties of boundary layer clouds: Droplet effective radius versus number concentration. *J. Atmos. Sci.* **57**, 803-821 (2000).
26. Shao, H. & Liu, G. Detecting drizzle in marine warm clouds using combined visible, infrared, and microwave satellite data. *J. Geophys. Res.* **109**, D07205 doi:07210.01029/02003JD004286 (2004 ).
27. Shao, H. & Liu, G. Why is satellite observed aerosol's indirect effect so variable? *Geophys. Res. Letts.* **32**, L15802, doi:15810.11029/12005GL023260 (2005).
28. (A) from Eqn. 1 of (15); (B) from Eqn. 2 of (16); (C) from Table 3 of (17); (D) from Eqn. 4 of (14) based on the dataset of (18); (E) from (19); (F) from Table 2 of (20); (G) from Table 3 of (21); (H) based on the data plotted in Fig. 3 of (22); (I) based on Eqns. (A), (B), and (C) for marine clouds of (13).

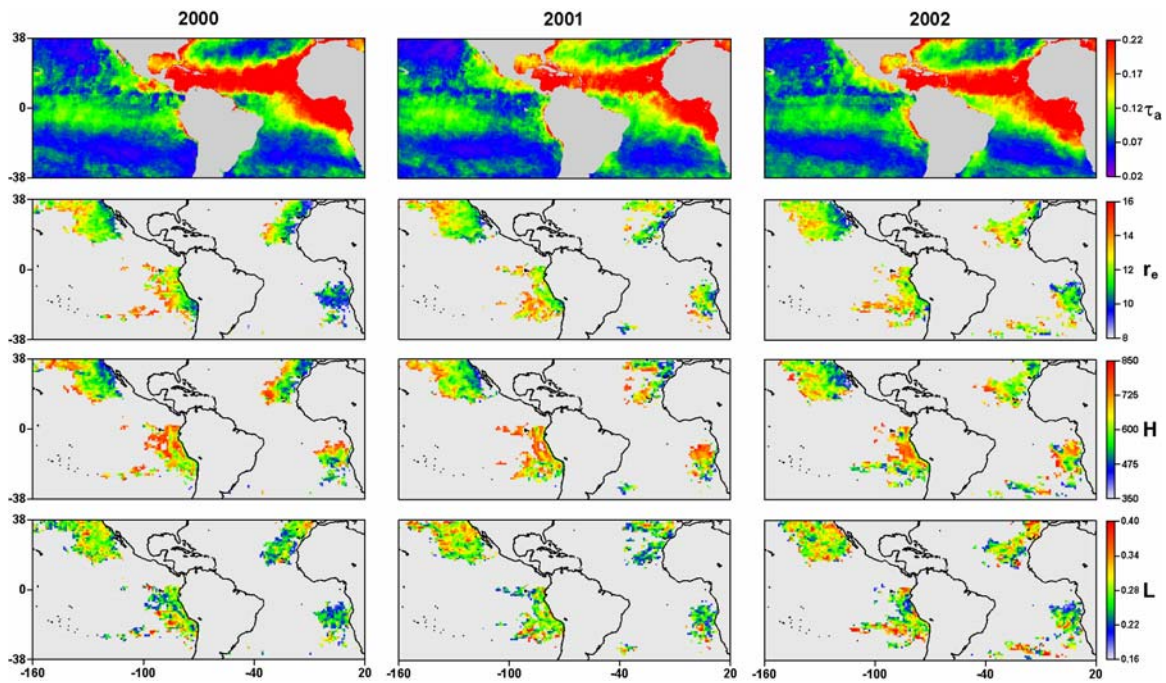


Fig. 1 Three-monthly (June to August)  $1^\circ$  by  $1^\circ$  geometric mean distributions of aerosol optical depth  $\tau_a$  over the ocean and cloud effective radius  $r_e$  ( $\mu\text{m}$ ), cloud geometric thickness  $H$  (m), and liquid water content  $L$  ( $\text{g m}^{-3}$ ) over the Eastern sub-tropic oceans during 2000 to 2002.

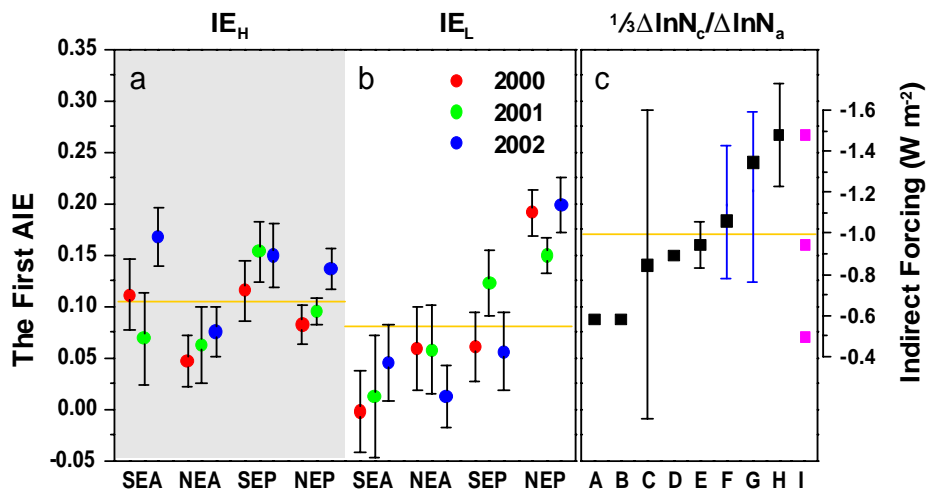


Fig. 2 the first aerosol indirect effect observed over the eastern side of the subtropical oceans during JJA of 2000 to 2002 with and without the correlation term (shadowed), and the in situ measurements from various investigators A-I<sup>28</sup>. The black error bars represent the 95% confidence intervals and the blue denote the range. The horizontal orange lines show the mean values. The right y-axis scale the indirect aerosol forcing based on the study of Boucher and Lohmann<sup>13</sup>, the points in magenta are their assumed responses of the cloud droplet concentrations to the sulphate aerosols over ocean.

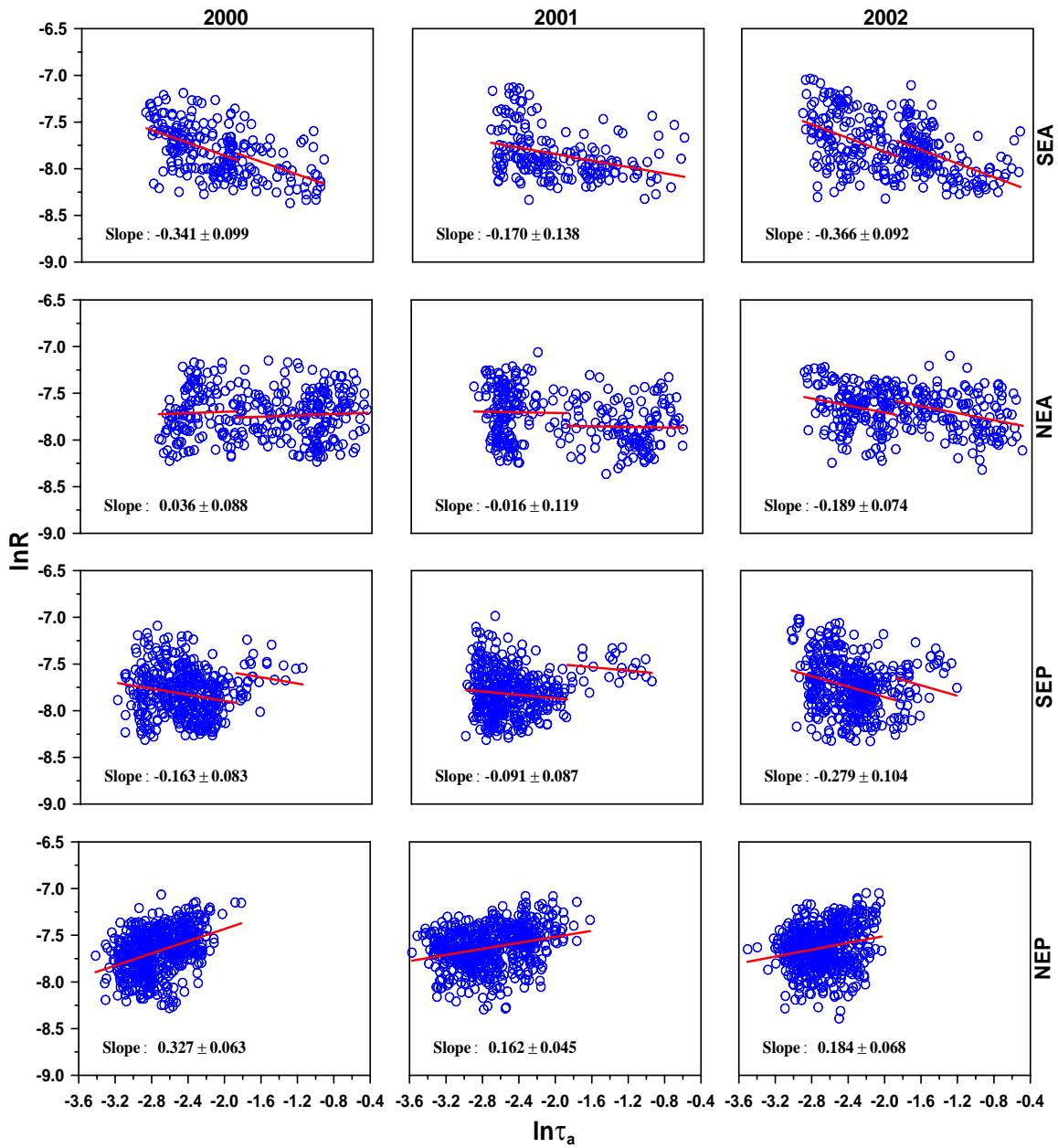


Fig. 3 the dependence of  $\ln R$  on  $\ln \tau_a$ . Red lines are the best fits. Legend shows the slope followed by 95% confidence interval.

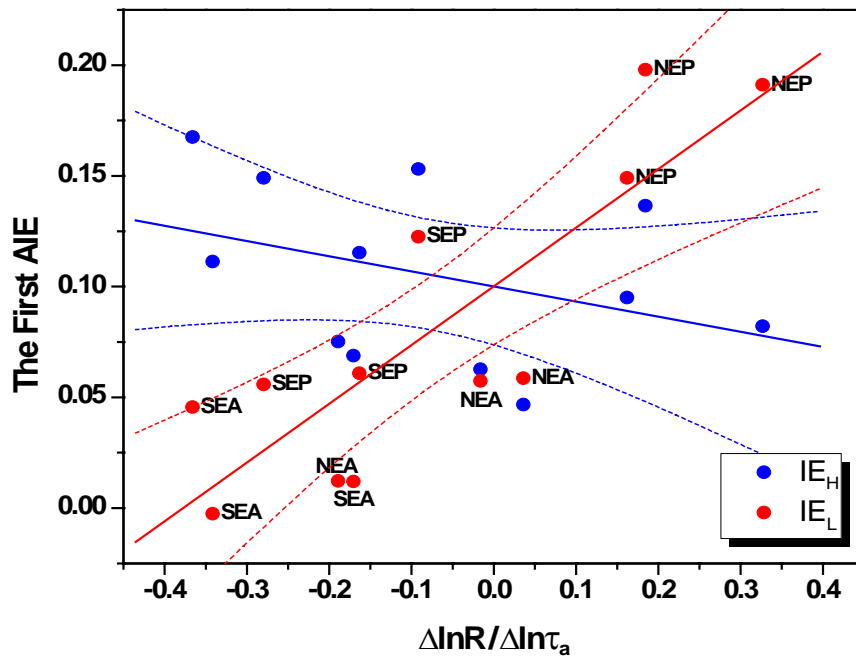


Fig. 4 the first AIEs measured by  $IE_H$  and  $IE_L$  as the function of the correlation between  $R$  and  $\tau_a$ .

Supplementary Information:

Most forward calculations of the first aerosol indirect radiative forcing in climate models are based on  $\Delta \ln N_c / \Delta \ln N_a$  or its surrogates, where  $N_c$  and  $N_a$  are cloud droplet and aerosol number concentrations, respectively; and  $\Delta$  means taking the difference of variables between clean and polluted clouds. Since natural clouds are subjected to mixing with their ambient drier air, leading to some cloud droplets being evaporated, the measured  $\Delta \ln N_c / \Delta \ln N_a$  can breakdown into two parts, i.e.,

$$\frac{\Delta \ln N_c}{\Delta \ln N_a} = \frac{\Delta \ln N'_c}{\Delta \ln N_a} + \frac{\Delta \ln R_N}{\Delta \ln N_a}, \quad (1)$$

where  $N'_c$  denotes the idealized cloud number concentration without undergone mixing;  $R_N$  is the ratio of  $N'_c$  to  $N_c$ . The first term on the right side of (1) indicates the change of cloud droplet number in response to the change of aerosol number concentration without the evaporation-induced reduction of cloud droplets. The second term on the right side of (1), however, is a term arising from the correlation between  $R_N$  and  $N_a$  within the group of clouds used for analysis. If  $N_a$  and  $R_N$  vary randomly or  $R_N$  is uniform within the group of clouds, the averaged value of the second term should be zero. Otherwise, if  $N_a$  and  $R_N$  vary in a coherent fashion within this group of clouds, a nonzero value will be resulted for this term, which can be negative or positive depending on the spatial distributions of  $R_N$  and  $N_a$ . Since the first aerosol indirect effect is meant to measure the change of cloud particle size due to aerosol variation without altering cloud liquid water content<sup>1</sup>, it should be estimated within the clouds that have the same  $R_N$ . In other words, the first aerosol indirect effect proposed by Twomey<sup>1</sup> should not be measured by  $\Delta \ln N_c / \Delta \ln N_a$ , but by  $\Delta \ln N'_c / \Delta \ln N_a$ .

For non-precipitating stratocumulus clouds, effective radius  $r_e$ , liquid water content at cloud top  $L$  and cloud number concentration  $N_c$  satisfy<sup>9</sup>:

$$r_e \propto \omega L^{1/3} N_c^{-1/3}, \quad (2)$$

where  $\omega$  is a non-dimensional parameter depicting the dispersion of cloud drop spectrum. Assuming  $R_L = L/L'$  (here the symbols with prime denote quantities for idealized non-evaporation), also considering  $L' \propto H$ , the depth of the cloud, we deduce the following relation from (2)

$$r_e \propto \omega (R_L H)^{1/3} N_c^{-1/3}. \quad (3)$$

From (1) to (3), noting  $\tau_a$  is a proxy of  $N_a^{S1}$ , we have

$$IE_L \equiv -\frac{\Delta \ln(r_e L^{-1/3})}{\Delta \ln \tau_a} = \frac{1}{3} \frac{\Delta \ln R_N}{\Delta \ln R_L} \cdot \frac{\Delta \ln R_L}{\Delta \ln \tau_a} + \frac{1}{3} \frac{\Delta \ln N'_c}{\Delta \ln \tau_a} - \frac{\Delta \ln \omega}{\Delta \ln \tau_a}, \quad (4)$$

and

$$IE_H \equiv -\frac{\Delta \ln(r_e H^{-1/3})}{\Delta \ln \tau_a} = \left( \frac{1}{3} \frac{\Delta \ln R_N}{\Delta \ln R_L} - \frac{1}{3} \right) \cdot \frac{\Delta \ln R_L}{\Delta \ln \tau_a} + \frac{1}{3} \frac{\Delta \ln N'_c}{\Delta \ln \tau_a} - \frac{\Delta \ln \omega}{\Delta \ln \tau_a}. \quad (5)$$

According to the homogeneous/inhomogeneous mixing concept<sup>S2-S4</sup>, the inhomogeneous mixing process decreases cloud droplet number concentration but without decreasing the mean volume radius (i.e.,  $N_c/N'_c = L/L'$ ), while the homogeneous mixing process decreases both cloud droplet number concentration and the mean volume radius (i.e.,  $N_c/N'_c > L/L'$ ). Since in stratocumulus clouds mixing process is dominated by the inhomogeneous process,  $\Delta \ln R_N/\Delta \ln R_L$  should be close to 1. Note that  $\Delta \ln R_L$  equals to  $\Delta \ln R$  (where,  $R=LH^{-1}$ ), our data confirms this. Actually our data shows that the ratio  $\Delta \ln R_N/\Delta \ln R_L$  is slightly smaller than 1 (ref. Fig. 4), possibly because the mixing is close to inhomogeneous process for coastal polluted clouds, but between homogeneous and inhomogeneous for clean clouds far off the coast. Therefore, the sensitivity of  $IE_L$  to  $\Delta \ln R_L/\Delta \ln \tau_a$  is close to 1/3 and that of  $IE_H$  is close to 0. In other words,  $IE_L$  and  $IE_H$  measure the first AIE with and approximately without the mixing influence, respectively.

Due to the different sensitivities to  $\Delta \ln R_L / \Delta \ln \tau_a$ , according to Eq. (4) and (5),  $IE_L$  equals to  $IE_H$  only when  $\Delta \ln R_L / \Delta \ln \tau_a$  is zero, i.e., when correlation term vanishes. Since an increase of aerosol loading leads to concurrent increases of droplet concentration and relative dispersion of the cloud droplet size distribution, we propose the first AIE should be a sum of the two competing effects arising from the change in droplet concentration and relative dispersion. Therefore, the first AIE should be measured by the sum of last two terms on the right side of (4) or (5). Recalling  $IE_L = IE_H$  when correlation term vanishes, the cross-point of  $IE_L$  and  $IE_H$  as functions of  $\Delta \ln R_L / \Delta \ln \tau_a$  (ref. Fig.4) represents the first AIE unbiased by mixing influence.

## Reference

- S1. Nakajima, T., Higurashi, A., Kawamoto, K. & Penner, J.E. A possible correlation between satellite-derived cloud and aerosol microphysical parameters. *Geophys. Res. Lett.* **28**, 1171-1174 (2001).
- S2. Burnet, F. & Brenguier, J.L. Observational study of the entrainment-mixing process in warm convective clouds. *J. Atmos. Sci.* (2006).
- S3. Baker, M.B., Corbin, R.G. & Latham, J. The influence of entrainment on the evolution of cloud droplet spectra: I. A model of inhomogeneous mixing. *Q. J. R. Meteorol. Soc.* **106**, 581-598 (1980).
- S4. Blyth, A.M. & Latham, J. A climatological parameterization for cumulus clouds. *J. Atmos. Sci.* **48**, 2367-2371 (1991).

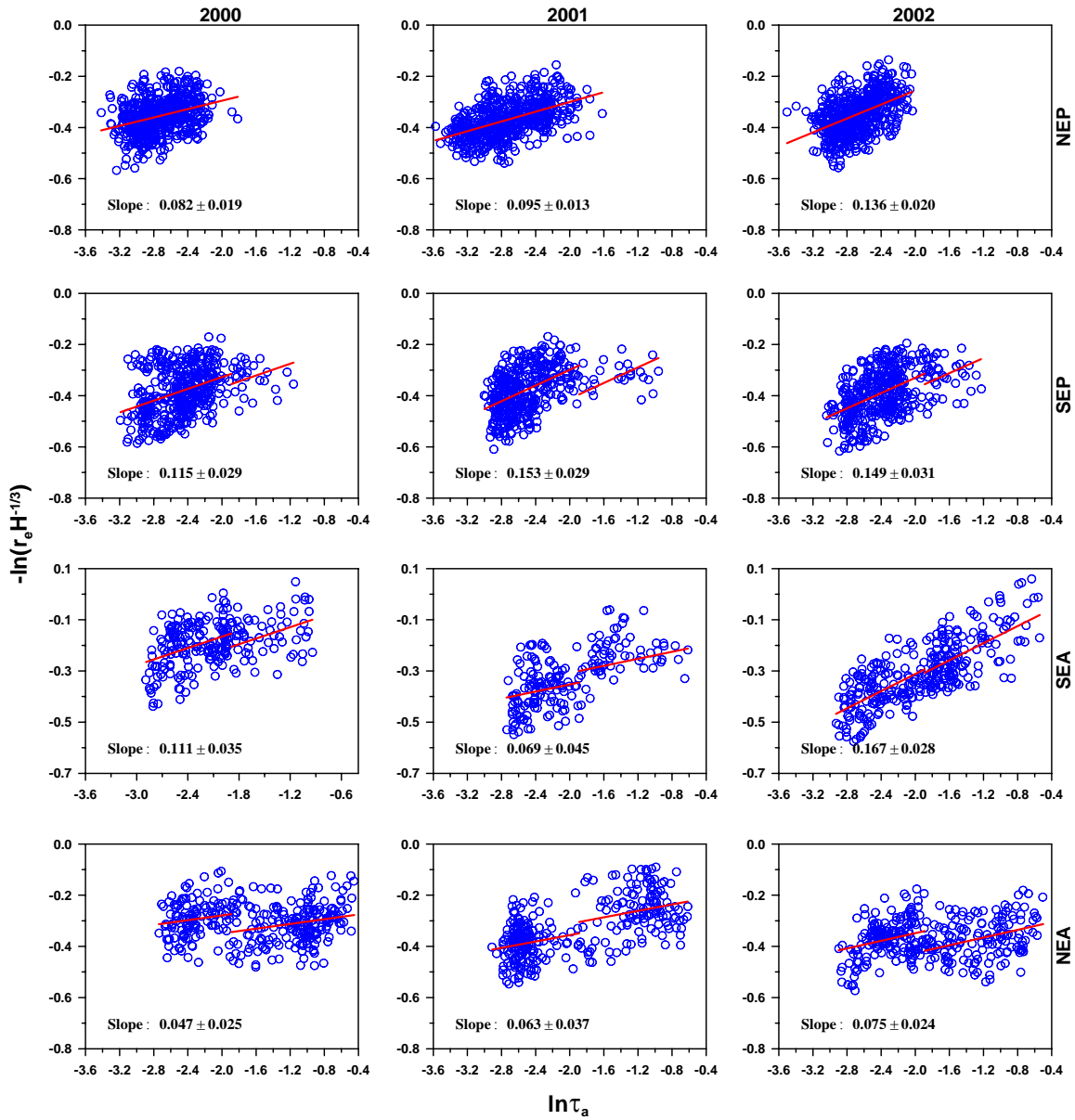


Fig. S1 The dependence of  $-\ln(r_e H^{-1/3})$  on  $\ln \tau_a$ . Red lines are the best fits. Legend shows the slope followed by 95% confidence interval.

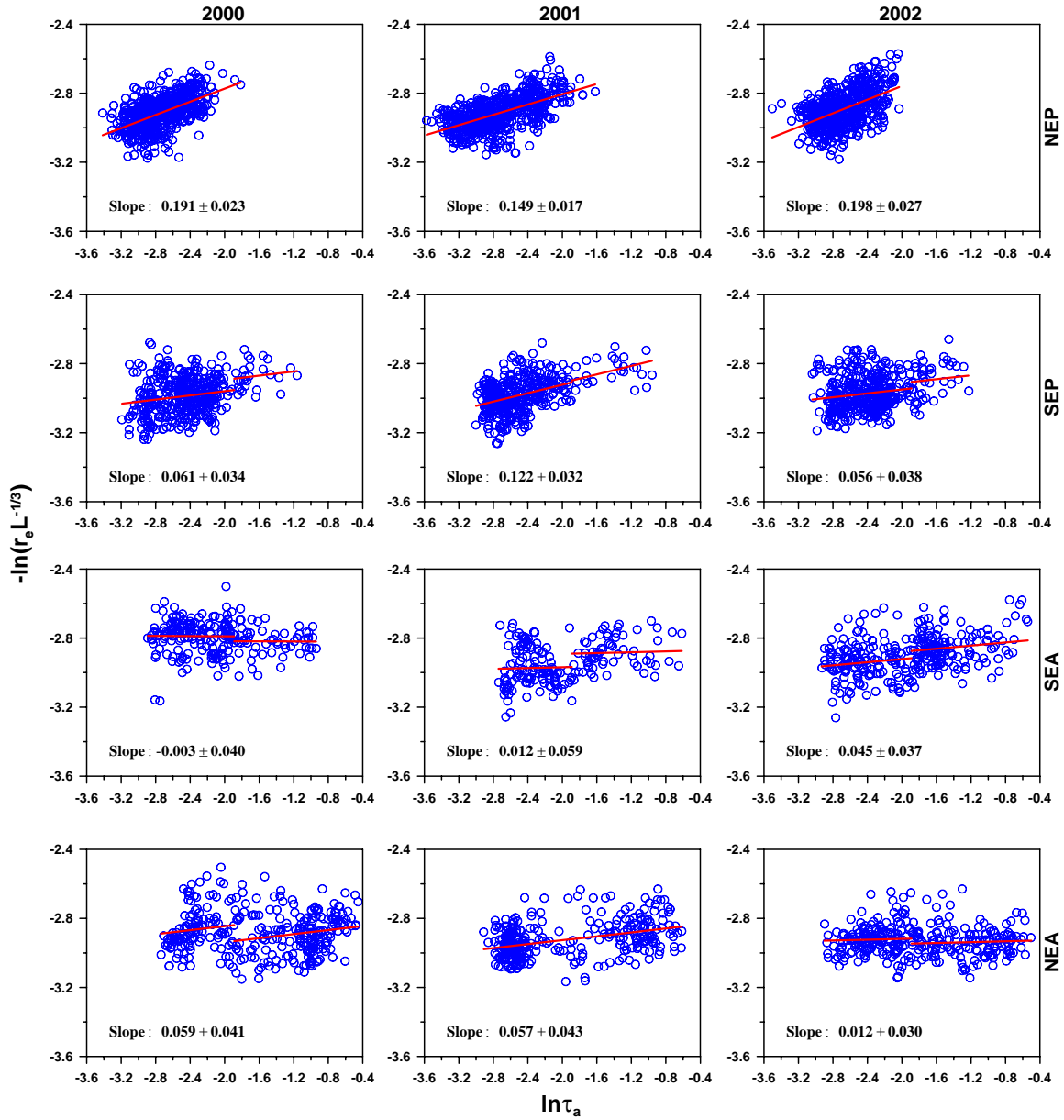


Fig. S2 The dependence of  $-\ln(r_e L^{-1/3})$  on  $\ln \tau_a$ . Red lines are the best fits. Legend shows the slope followed by 95% confidence interval.